Remote Sensing of Environment 113 (2009) 907–918

Contents lists available at ScienceDirect

Remote Sensing of Environment

journal homepage: www.elsevier.com/locate/rse

The behaviour of snow and snow-free surface reflectance in boreal forests: Implications to the performance of snow covered area monitoring

Miia Salminen [a], Jouni Pulliainen [b], Sari Metsämäki [a,*], Anna Kontu [b], Hanne Suokanerva [b]

[a] Finnish Environment Institute, Geoinformatics and Land Use Division, P.O.Box 140, FI-00251 Helsinki, Finland
[b] Finnish Meteorological Institute, Arctic Research, Tähteläntie 62, 99600 Sodankylä, Finland

ARTICLE INFO

Article history:
Received 28 May 2008
Received in revised form 15 December 2008
Accepted 16 December 2008

Keywords:
Snow cover
Surface reflectance
Field spectroscopy
Boreal forest

ABSTRACT

Optical methods for snow mapping typically exploit wavelengths in the visible and near-infrared range, where reflectances from snow and snow-free ground may significantly vary, especially during the melting season. In this study, the variability of ground reflectance in the boreal forest zone was investigated in order to assess the feasibility of satellite sensors to the mapping of snow covered area (SCA). This aims at the improvement of the existing snow mapping algorithms, such as the reflectance model-based snow monitoring method *SCAmod* of the Finnish Environment Institute (SYKE). We acquired and identified some statistical features for reflectance spectra of seasonally snow covered and snow-free terrain by using a field spectroradiometer (ASD Field Spec Pro JR). Extensive measurement campaigns were carried out in 2007–2008 in northern Finland, resulting to hundreds of spectral samples between 350 and 2500 nm. The main emphasis was put on the determination of the melting snow reflectance under different weather conditions and stages of snow metamorphosis as well as over different terrain types. The gained reflectance spectra provide useful information for optical snow mapping studies in general. In this investigation, the primary function of the spectrometer data was the accuracy assessment and optimal band selection when applying the *SCAmod*-method to different space-borne instruments (MODIS, MERIS and AVHRR). The correspondence of small scale field observations with scene reflectance was also addressed. This was performed by comparing field spectrometer data with mast-based observations.

Based on the inversibility of the *SCAmod* reflectance model, we addressed the standard deviation (standard error) of SCA estimation contributed by wet snow and snow-free ground reflectance fluctuations. An average error in the determination of the fractional Snow Covered Area (SCA) of about 5–7 %-units was obtained (range from 0% = snow-free ground to 100% = full snow cover), the maximum error of 10–12 %-units occurring at full snow cover conditions (for the moment when first open patches are emerging). These investigations show that the variability in the reflectances of snow and snow-free ground is a significant error source in snow mapping. However, providing the SCA with descriptive error statistics is very beneficial for further use as the error statistics are needed for data assimilation approaches, e.g. in using SCA-values as input to hydrological models.

1. Introduction

The Northern Hemisphere seasonal snow cover influences highly the interactive Earth's surface and atmosphere system. For this reason, snow cover is a sensitive climate change indicator both regionally and on global scale. Typically, at northern latitudes most of the annual discharge originates from snowfall. Consequently, snow pack is also an important temporary fresh water storage. Terrestrial snow cover is a rapidly varying constituent of the hydrological cycle in particular during the spring and autumn transition months (Barry et al., 2007; Vavrus, 2007; Walsh, 2005). Spatial variability and long-term trends in snow cover distribution and related climate patterns have been analyzed based on observation data (Kitaev et al., 2002, 2005) and climate change prediction models (Jylhä et al., 2004; Mellander et al., 2007). The models project changes in the spatial and temporal distribution of snow in the boreal forest zone. Although the predictions generally indicate significant decrease in snow cover throughout the winter and the acceleration of the hydrologic cycle, the amount of snow increases in the coldest areas, such as the Canadian Arctic and Siberia (Räisänen, 2008). These changes can have widespread impacts on ecosystems and human activities, e.g. flooding, water resources management, agriculture, transportation, hydropower production, and recreational activities (Barry et al., 2007; Jaagus, 1997; Walsh, 2005). Accurate information on snow spatial and temporal distribution is essential for climate research, numerical

* Corresponding author.
E-mail address: sari.metsamaki@ymparisto.fi (S. Metsämäki).

0034-4257/$ – see front matter © 2008 Elsevier Inc. All rights reserved.
doi:10.1016/j.rse.2008.12.008

weather prediction and hydrological applications. Lundberg and Halldin (2001) review and assess ground-based snow measurement techniques for boreal areas and state the importance of both point and remote sensing observations.

Traditional in-situ weather station and snow-gauging networks are in practice handicapped by their spatial and temporal sparseness. Space-borne Earth Observation (EO) techniques provide a spatially and temporally effective means to obtain information on the snow cover extent, including the fraction of snow covered area (SCA) within a single pixel or a single calculation unit such as a hydrological drainage basin. Optical snow mapping methods are often based on the fact that snow has high reflectance in visible and near infrared (NIR) wavelengths compared to most other land surfaces (Warren, 1982; Wiscombe & Warren, 1980). This difference is used in operational snow cover monitoring systems, such as the National Oceanic and Atmospheric Administration (NOAA) snow map production for the Northern Hemisphere, fractional snow cover mapping for the Baltic Sea area with *SCAmod* (Metsämäki et al., 2005) and the retrieval of the global Moderate Resolution Imaging Spectroradiometer (MODIS) snow-cover products (Hall et al., 2002). The MODIS algorithm employs visible green and shortwave-infrared reflectances to calculate the Normalized Difference Snow Index (NDSI), which is used to provide either binary snow information (snow/no snow) or fractional SCA based on regression analysis between NDSI and Landsat 30-m observations used as "ground truth" (Salomonson & Appel, 2004). Additionally, linear spectral unmixing techniques have been applied for sub-pixel snow mapping by assuming that a pixel is composed of several spectral classes. (Nolin & Dozier, 1993; Painter et al., 1998, 2003; Rosenthal, 1996; Vikhamar & Solberg, 2003a,b). Spectral unmixing is specifically suitable for data with a considerable number of spectral bands, such as Airborne Visible/Infrared Imaging Spectrometer (AVIRIS), but less usable in remote sensing of snow with current space-borne instruments with limited number of bands (MODIS, AVHRR, MERIS). Using spectral unmixing approach, the aerial coverage of each class can be estimated. Unmixing often utilizes spectral libraries for comparison to estimate the mixture spectral endmembers i.e. pure spectral classes of each pixel. For that purpose, the spectra obtained from this investigation can be exploited and are relevant with instruments such as AVIRIS, although the study does not directly concern spectral unmixing.

There are characteristic sources of error for different satellite data retrieval methods caused by the spatial and temporal variation in the observed reflectance. In order to quantify the effects of this variation on the SCA estimation, measurements under controlled conditions are fundamental. The variation in the observed reflectance can be compiled to statistics by collecting reference spectra with field spectroscopy measurements performed at ground level. Field spectroscopy advances remote sensing (imaging spectroscopy) through feasibility studies, image analysis and vicarious calibration of satellite products (Schaepman et al., 2006). For example, the retrieval of optically equivalent snow grain size is at present only possible by utilizing high spectral resolution spectroscopy data (Painter & Dozier, 2004; Painter et al., 1998). Previous investigations concerning the behaviour of surface reflectance also include the employment of simulated spectra based on theoretical models (Nolin & Dozier, 2000; Wiscombe & Warren, 1980). Problems in theoretical investigations include that they often consider snow grains as spherical scatterers. This adduces the difficulty of determining the effective grain radius for real non-spherical snow crystals, or otherwise, how to describe non-spherical shapes for more advanced models (Kokhanovsky et al., 2005; Painter & Dozier, 2004; Xie et al., 2006).

In this work, we study the variability of surface reflectance in the boreal forest area in order to enable the improvement of existing optical EO-based snow mapping algorithms, such as the reflectance model-based *SCAmod* method (Metsämäki et al., 2005) developed and operated at the Finnish Environment Institute (SYKE). *SCAmod* is particularly designed for boreal forests, excluding mountainous areas (Anttila et al., 2005). It provides the fraction of Snow Covered Area (SCA) during the melting season, presented as average percentages (0–100%) for calculation unit areas. These can be drainage basins or grid cells equivalent to the satellite pixel size. The operational snow mapping at SYKE is currently based on 500-meter resolution Terra/MODIS-imagery. The *SCAmod* algorithm is based on a single band reflectance model, where the observed satellite reflectance for a selected wavelength channel is expressed as a function of SCA. The typical reflectance values, again for the selected wavelength band, of three major reflective contributors (wet snow, snow-free ground, and dense forest canopy) serve as input parameters. *SCAmod* is, however, applicable to a variety of optical sensors; switching between sensors only requires tuning the values of the constant parameters of the algorithm. These are (a) reflectance of wet snow cover, (b) reflectance of snow-free ground and (c) reflectance of forest canopy (crowns and trunks). In addition to those, dry snow reflectance must be concerned as it affects at-satellite reflectance-derived apparent forest canopy transmissivity, which is *a priori* information required by *SCAmod* and is based on the same reflectance model as the actual SCA estimate. The snow information provided by SYKE is primarily used for hydropower management and hydrological modelling (Metsämäki et al., 2004). The principle of the *SCAmod* method is described in Section 2.4.

We consider here the accuracy of the above-described *SCAmod* method using ground spectrometer-derived average reflectances as input to *SCAmod* at applied satellite-sensor-specific wavelengths. As *SCAmod* is based on a reflectance model and applies typical average reflectances, contributions (a)–(c) above, as input parameters, a critical error source must be related to the presumed absolute level and variation in these reflectance values. Since *SCAmod* uses single band reflectances, we concentrated on selected wavelength bands in our analyses. However, the data set introduced here is also relevant in general, e.g. for approaches that use a wide range of spectrum, such as that by Painter et al. (2003). An essential issue here is to investigate the variability of snow and snow-free surface reflectances, particularly under different state of snow metamorphosis, within several land-cover categories and under various weather and illumination conditions. The current paper concentrates on the effects of wet snow and snow-free ground reflectance variability to the *SCAmod* algorithm performance as we assume their effect to be more significant compared to more invariant dry snow and forest canopy reflectance.

In order to investigate the scene reflectance contributions indicated above, we collected an extensive field spectrum data set using a portable spectroradiometer (ASD Field Spec Pro JR) in 2007 and 2008 in Finnish Lapland. The obtained spectral data was divided into selected reflectance classes for which mean and standard deviation were calculated. Another similar spectrometer was permanently installed in a 30-m mast providing data for a pine forest and open terrain (partially shadowed by pine trees). The comparison of field and mast spectrometer observations enabled the investigation how well the scene reflectance observed by a space-borne system can be modelled using point-wise observed field spectrometer data.

To perform the actual accuracy assessment of *SCAmod*, we calculate the contributions of both wet snow and snow-free ground reflectance fluctuations to the standard deviation (standard error) of an SCA estimate. The goal of analyses is to investigate the temporal and spatial variability in the average reflectances and to find out their effect to performance of SCA estimation. The gained estimates for the variance of snow covered and snow-free terrain reflectance directly provide information for the future *SCAmod* algorithm modification as well as for error analyses. The objective also includes the study of the dependence of wet snow reflectance on depth of the snowpack. Furthermore, optimal band alternatives are indicated for current and future satellite instruments by determining the wavelength areas where the variability is only minor or has only a slight effect on the performance of a snow covered area algorithm. In this study, we focus

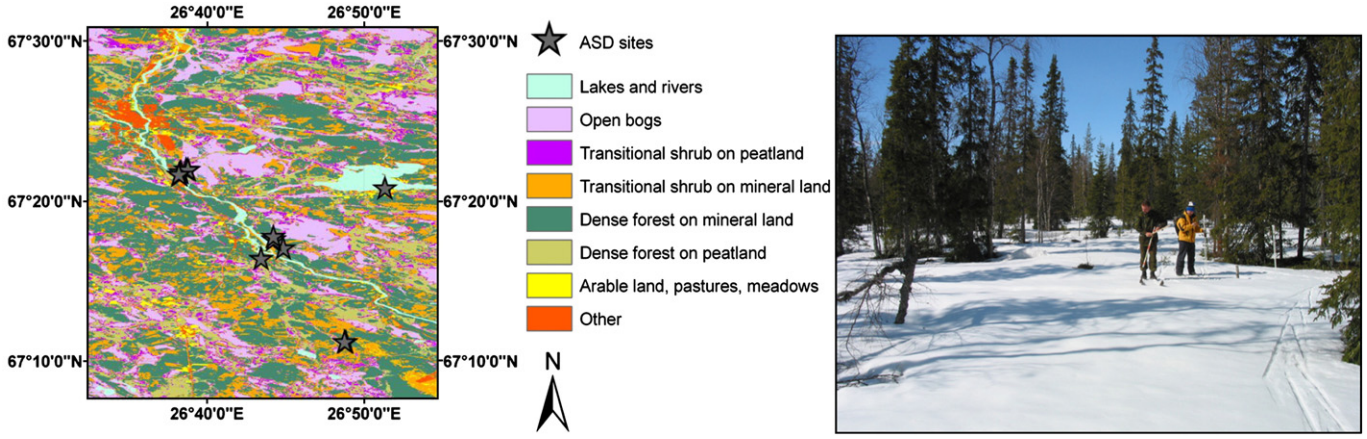

Fig. 1. (Left) The reflectance sites are located in Sodankylä and Inari districts in Finnish Lapland, an additional site was located in an open fjeld region north of the map region. (Right) Typically, the landscape represents an open canopy conifer-dominated boreal forest.

on wavelength areas related to three satellite sensors commonly used in snow mapping: the MODIS aboard Terra, the Medium Resolution Imaging Spectrometer (MERIS) aboard Envisat and the Advanced Very High Resolution Radiometer (AVHRR) aboard NOAA satellite series.

2. Data set and methods

2.1. Study area

The target area for fieldwork is in the Sodankylä district in Finnish Lapland, located on latitude 67 N about 100 km north of the Arctic Circle (Fig. 1). This sub-arctic environment is characterized by seasonally snow covered boreal coniferous forests and large open bogs or sparsely forested mires. Typical for the terrain in Lapland are numerous tundra-like treeless fjelds, although the overall topography is relatively flat. The Sodankylä region is undulating moderately up to 500 m in altitude. The extent of forests (forests and scrubland) in Finland is 74% of the total land area compared to the 44% in Europe (FAO, 2003). In Finnish Lapland the areal extent of forest is 73%, but forests are sparse with an average stem volume of only 64 m^3/ha on forestland (METLA, 2007). Dominant tree species are Scots pine (76% of the forestland coverage) and Norway spruce, but small birches are also usual especially at fjeld-regions.

The most active period regarding snow hydrology is spring when the seasonal snow melts, often causing severe flooding particularly in the North. Snow characteristics of Finnish Lapland are more homogeneous compared to Southern Finland, where the repeated freezing and thawing usually result into a highly metamorphosed snowpack. In Finnish Lapland snow cover period tends to last more than 6 months in open areas and the average annual snow water equivalent is as high as 140–200 mm (Kuusisto, 1984). The structure of snowpack depends mainly on solar irradiation, air temperature, wind speed and rainfall that determine the type of metamorphosis process (Colbeck et al., 1990; Oksanen, 1999; Sturm et al., 1995). During spring melt metamorphosis, snowpack is typically structured with layers that may contain ice lenses or refrozen particles. In the Sodankylä region taiga type snow is predominant, but there is also tundra type snow, particularly on top of wind-induced fjelds. Fig. 1 depicts the location of the reflectance sites and indicates the high spatial heterogeneity of the landscape of the region.

2.2. Data acquisition

The overall strategy of the field measurements is to collect spatially and temporally extensive data sets that are needed for analysing the performance and error characteristics of SCA mapping. In addition, by combining spatially extensive point-wise (very small footprint) measurements with mast-based (185 m^2 footprint) experiments at a single location, we can then link the ground-based ASD measurements also to scene reflectances actually observed by space-borne remote sensing systems. Hundreds of reflectance spectra were sampled at the Sodankylä area in Finnish Lapland with a portable spectrometer (Analytical Spectral Devices (ASD) Field Spec Pro JR, spectral range 350–2500 nm). The purpose of the ASD measurements was to determine the reflectance variability of snow and snow-free ground. In order to identify and locate the most typical land cover categories, CORINE2000 Land Cover (CLC2000) map was used (Härmä et al., 2004). We found that open peat bog, transitional shrub on mineral or peat land and coniferous forest on mineral or peat land are the most typical land cover categories in the area (Fig. 1). Among those, several representative reflectance measurement sites were selected.

In addition to using the portable spectrometer, a similar spectrometer was installed on a top of a 30-m mast to constantly monitor reflectance of a target area including a Scots pine forest with a mean tree height of 7 m (stem volume 70 m^3/ha) and an adjacent forest opening. Same observation settings as with the portable spectrometer were used, except that the instrument was tilted 11° off the nadir. The main mast-borne data of this study was acquired for a single date, 27 March 2008. Additional data representing snow-free free conditions were used in order to find out the reference value for vegetation reflectance (multiple observations of the forested target area from August 2006). The mast-based spectrometer system is described in (Sukuvaara et al., 2007).

Simultaneously with mast-based spectrometer observations on March 2008, digital photographs were acquired for the target area enabling the determination of the fractions of forest canopy, tree shadows and directly illuminated snow surface (an automatic camera system is installed to mast-top together with the azimuthally rotating spectrometer front-end). In case of winter-time measurements this is possible as the visible contrast between different target composites is high. Analogously to ground-based observations, the mast-based reflected radiance observations were calibrated to reflectance values applying white reference panel measurements with an automatic mast-top calibration system.

Field campaigns in 2007 and 2008 consist of reflectance and concurrent snow measurements in 36 sites (each including 3–5 subsampling sites) from the time period of March to May, both in 2007 and 2008. Additional monitoring was carried out using the mast-based spectrometer system. Snow pits were excavated at each reflectance site and average snow depth, snow pack temperature (at −5 cm and middle of snowpack), ground surface temperature and air temperature were measured. Based on the temperature measurements and the so-called snowball test suggested by Colbeck et al.

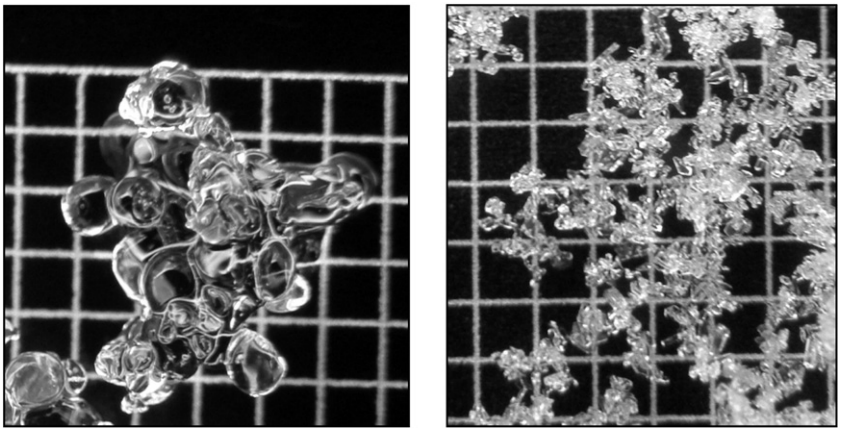

Fig. 2. (Left) Example of typical wet snow grains with 1 mm grid at the background. (Right) Example of typical dry snow grains with 1 mm grid at the background. The grain sizes range from 1.0 to 1.5 mm (mean of maximum diameter) for wet snow, 1.0 mm being the dominant grain size. Dry snow grain sizes range from 0.3 mm to 0.8 mm, the dominant size being 0.5 mm.

(1990), the surface snow layer was defined either dry or wet. Various reflectance cases from snow-free ground to snow depths up to 84 cm were recorded. The optically equivalent snow grain size was visually estimated by comparing a snow sample to a snow crystal screen with 1, 2 and 3-mm-grids, see Fig. 2. If the grain sample's average maximum diameter size was larger than 1 mm, the average value was estimated with a precision of 0.5 mm. With grains smaller than 1 mm, a precision of 0.25 was used. In cases with a mixture of different grain sizes, the range of sizes was recorded, but the typical or average value was used for the whole layer. From each range of sizes, outliers were excluded from the results by visual inspection. The obtained snow grain average maximum diameter sizes ranged between 0.2–2 mm for dry snow and 0.5–3.5 mm for wet snow, respectively. This method was found practical; although more advanced methods can be found from the literature (e.g. Aoki et al., 2000; Matzl & Schneebeli, 2006; Painter et al., 2007). The prevailing solar illumination conditions were visually determined to be either direct i.e. clear (0/8 to 2/8 cloud cover), diffuse i.e. cloudy (6/8 to 8/8 cloud cover) or varying conditions (3/8 to 5/8 cloud cover). Finally, digital photographs were taken from each snow sample and the surrounding environment for possible reanalysis, see Fig. 2. Table 1 summarizes snow, weather and environmental conditions during the measurements.

At the reflectance measurement sites, ground spectrometer-based spectra of wet snow, dry snow and snow-free ground were measured under various weather and sun illumination conditions and at different stages of snow metamorphosis. Generally we followed similar measurement pattern at each site with respect to measurement geometry, sampling strategy and calibration. The instrument foreoptic unit (measurement head) was set to look at nadir (0°) direction with 25° field of view (FOV). The angular anisotropy of the target reflectance was not specifically observed in this investigation. As the measurement head was mounted on a tripod at the height of around 45 cm, it was looking at a surface illumination area of 20 cm diameter. Approximately 90% of the ground-based observations were obtained with 50°–75° sun zenith angle range. Table 2 summarizes the measurement setup for spectrometer observations. Also the key characteristics of mast-borne ASD-observations are listed in Table 2. It should be noted that in northern latitudes during the winter and at the beginning of the snow melt season, solar zenith angles at solar noon are large (>50°).

It is necessary to observe the radiance (W m-2 sr-1 nm-1) reflected from the target and Lambertian standard reference to obtain the reflectance. Calibrated white reference optical panel with known reflectance spectrum was used as a reference (also in the mast-based system). During the calibration, the panel was placed horizontally above the snow surface close to the field of view of the spectrometer in a way that it is consistently under illumination. The calibration was carried out after each measurement series or whenever the illumination or weather conditions changed. Solar irradiation was also measured for each data series with cosine receptor for reanalysis.

The obtained ASD reflectance quantities approximate generally two different measurable reflectance quantities defined by Schaepman-Strub et al. (2006), see Fig. 3. As the used spectrometer has a 25° FOV and the data have been collected under clear (direct) and cloudy (diffuse) solar illumination conditions, the obtained ground spectra approximate the biconical reflectance factor and the hemispherical–conical reflectance factor. Here these quantities are referred to as ASD reflectances in a way that the biconical quantity relates to conditions where irradiance composes mostly of direct component (direct) and the hemispherical–conical quantity relates to cloudy conditions

Table 1
Weather and snow conditions for dry and wet snow reflectance acquisitions.

Parameter	Dry snow spectra		Wet snow spectra		Dry snow spectra in shadow		Wet snow spectra in shadow	
	Min	Max	Min	Max	Min	Max	Min	Max
Air temperature range (°C)	−10.0	+3.7	−2.4	+10.3	−10.0	−0.7	−2.4	+5.5
Snow surface temperature range (°C)	−10.5	−0.8	−2.3	+1.5	−10.5	−1.0	−2.3	+0.5
Snow depth range (cm)	54	84	0.5	73	55	84	45	70
Snow grain size range (mm) (mean of max. diameter)	0.2	2	0.5	3.5	0.2	1.5	0.5	3.5
No. of diffuse/direct reflectance sites[a]	3/5		15/11		−/3		−/6	

Field work period lasted from March to May during 2007 and 2008 consisting of 36 reflectance sites measured in 14 separate days.

[a] 2 of the total of 36 in-situ sites were rejected due to varying illumination conditions; some sites include both direct and diffuse illumination cases.

Table 2
Characteristics of ASD instrumentation and measurement set-up.

Parameter	Ground ASD value	Mast ASD value
Spectrum	350–2500 nm	350–2500 nm
Sampling interval	1.4 nm for 350–1000 nm, 2 nm for 1000–2500 nm	1.4 nm for 350–1000 nm, 2 nm for 1000–2500 nm
Calibration	Spectralon® white panel with known reflectance	Spectralon® white panel with known reflectance
Field of view (FOV)	25° bare fibre	25° bare fibre
View angle direction	0° i.e. nadir	11° (8° in Aug. 2006)
Average footprint diameter/size	20 cm	185 m^2
FOV mean distance to target	45 cm	33 m

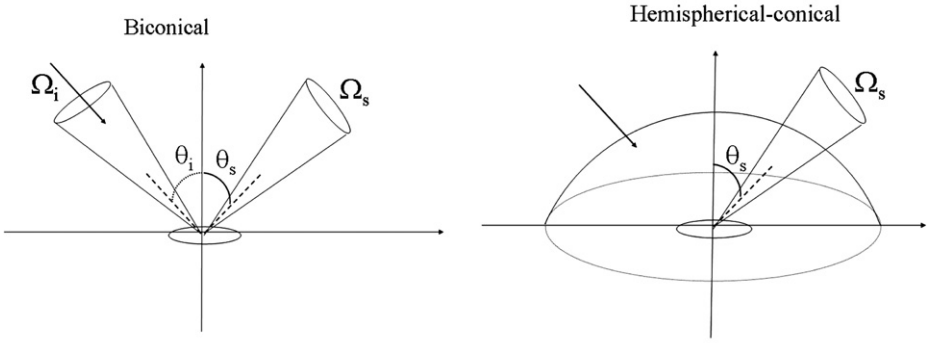

Fig. 3. (Left) Biconical reflectance factor here referred to as the direct ASD reflectance obtained in clear sky conditions and (Right) the hemispherical–conical reflectance factor here referred to as diffuse ASD reflectance obtained in cloudy conditions. θ_i denotes the sun zenith angle and θ_s the observation angle. Definitions and images are according to (Schaepman-Strub et al., 2006).

where irradiance has mainly diffuse components (diffuse). This is an approximation because in natural conditions the irradiance is not completely hemispherical even in uniformly cloudy weather. In the direct case the Sun disc is the conical source of illumination (almost directional). To be exact, the reflectance under clear skies approximates the biconical case better at the longer wavelengths. At shorter wavelengths, where the diffuse irradiance component is stronger and nontrivial, the reflectance then includes contributions representing both biconical and hemispherical–conical cases. The observed reflectance factor quantities can have values above 1 as the reflected radiation to a certain direction can exceed that of the Lambertian surface. The diffuse ASD reflectance is a quantity that approximates the hemispherical–directional reflectance factor (HDRF), whereas the direct ASD reflectance approximates the bidirectional reflectance factor (BRF) even though the instantaneous FOV of the instrument is 25° (in practice we assume that the reflectance is uniform across that FOV). Satellite instruments are often referred to observe BRF that can be used to estimate the actual surface reflectance (i.e. directional to hemispherical reflectance), typically using the crude assumption that the Earth's surface would be Lambertian.

Analogously to Schaepman-Strub et al. (2006), we can define the equation of BRF and HDRF as:

$$\mathrm{BRF} = \pi \cdot f_s(\theta_i, \varphi_i, \theta_s, \varphi_s; \lambda) = \pi \frac{L(\theta_i, \varphi_i, \theta_s, \varphi_s; \lambda)}{E_i(\lambda)} \quad (1)$$

where the incoming (projected to horizontal level) irradiance $E_i(\lambda) = E_0(\theta_i, \varphi_i; \lambda) \cos\theta_i$, E_0 is the incoming irradiance, L is the reflected radiance and f is the BRDF (bidirectional reflectance distribution function). θ_i and φ_i denote sun zenith angle and sun azimuth angle, respectively; θ_s and φ_s denote view zenith angle and view azimuth angle, respectively.

In case of HDRF irradiance is predominantly a hemispherically isotropic quantity and thus

$$\mathrm{HDRF} = \mathrm{BRF} \cdot d + (1-d) \int_0^{2\pi} \int_0^{\frac{\pi}{2}} f_s(\theta_i, \varphi_i, \theta_s, \varphi_s; \lambda) \cos\theta_i \sin\theta_i d\theta_i d\varphi_i \quad (2)$$

where d is the fraction of direct radiant flux.

The absolute accuracy of the reflectance data presented here depends upon the calibration carried out using the white reference panel. In practice, the anisotropic bidirectional reflectance factor of spectralon panel affects the absolute calibration accuracy, especially for the measurement of BRF under clear sky conditions for high zenith angles. We estimated the maximum possible error arising from this in our case by applying data on spectralon BRF presented by Sandmeier et al. (1998). The analysis indicated that at the wavelength band of 459–479 nm, the values reported for reflectance under direct solar illumination conditions, for the very high solar zenith angles of 75°, can be overestimated at the highest of about 6% (assuming that no diffuse irradiance component is present, $d = 1$ in Eq. (2)). In case of ideally diffuse conditions $d = 0$ in Eq. (2). Then the resulting overestimation at the band of 459–479 nm can be at the highest of about 4%, respectively.

2.3. Evaluation of snow reflectance and scene reflectance

Eventually, 36 different ground targets were measured the selection being based on snow properties (snow depth, snow wetness, snow grain size, snow metamorphosis stage and impurity (mainly forest litter) content), target type, illumination conditions, forest shading and land cover type. The selected ground targets' standard deviation and mean are composed of from several dozens up to around 1500 individual spectra at 350–2500 nm. Additionally, reflectances related to selected satellite sensor bands were extracted for *SCAmod* accuracy analysis and method development. These data were classified to represent the following general cases (both for direct and diffuse illumination):

- wet snow (average of all sub-cases)
- dry snow (average of all sub-cases)
- snow-free ground (average for different soil types directly after the snow melt: open bogs, other peat lands, mineral soil sites)
- wet snow in forest shadow (only for direct illumination conditions)
- dry snow in forest shadow (only for direct illumination conditions)
- wet snow, snow depth >20 cm
- wet snow, snow depth <20 cm.

The mast-based spectrometer observations representing both the open and forested area were compared against ground-based snow reflectance measurements. The applied ground-based reflectance data include observations from directly illuminated and shadowed snow surfaces (shadowed by tree trunks and crowns). In practice, a linear mixing model was used to describe the tower-based observations as a function of ground-based ASD-reflectances in cases of the open target area Eq. (3a) and the forested area Eq. (3b):

$$\begin{cases} R_{\lambda,\mathrm{obs}} = F_{\mathrm{direct}}\rho_{\lambda,\mathrm{snow}} + (1 - F_{\mathrm{direct}})\rho_{\lambda,\mathrm{shadow}} & (3a) \\ R_{\lambda,\mathrm{obs}} = F_{\mathrm{direct}}\rho_{\lambda,\mathrm{snow}} + (1 - F_{\mathrm{direct}} - F_{\mathrm{trees}})\rho_{\lambda,\mathrm{shadow}} + F_{\mathrm{trees}}\rho_{\lambda,\mathrm{trees}} & (3b) \end{cases}$$

where $R_{\lambda,\mathrm{obs}}$ is the scene reflectance simulated by ground-based observations, F_{direct} is the areal fraction of directly illuminated area, $\rho_{\lambda,\mathrm{snow}}$ is the reflectance of directly illuminated snow and $\rho_{\lambda,\mathrm{shadow}}$ is the reflectance of snow in shadow (calibrated to downwelling irradiance at non-shadowed conditions). F_{trees} is the fraction of tree crowns and trunks in the mast-borne reflectance

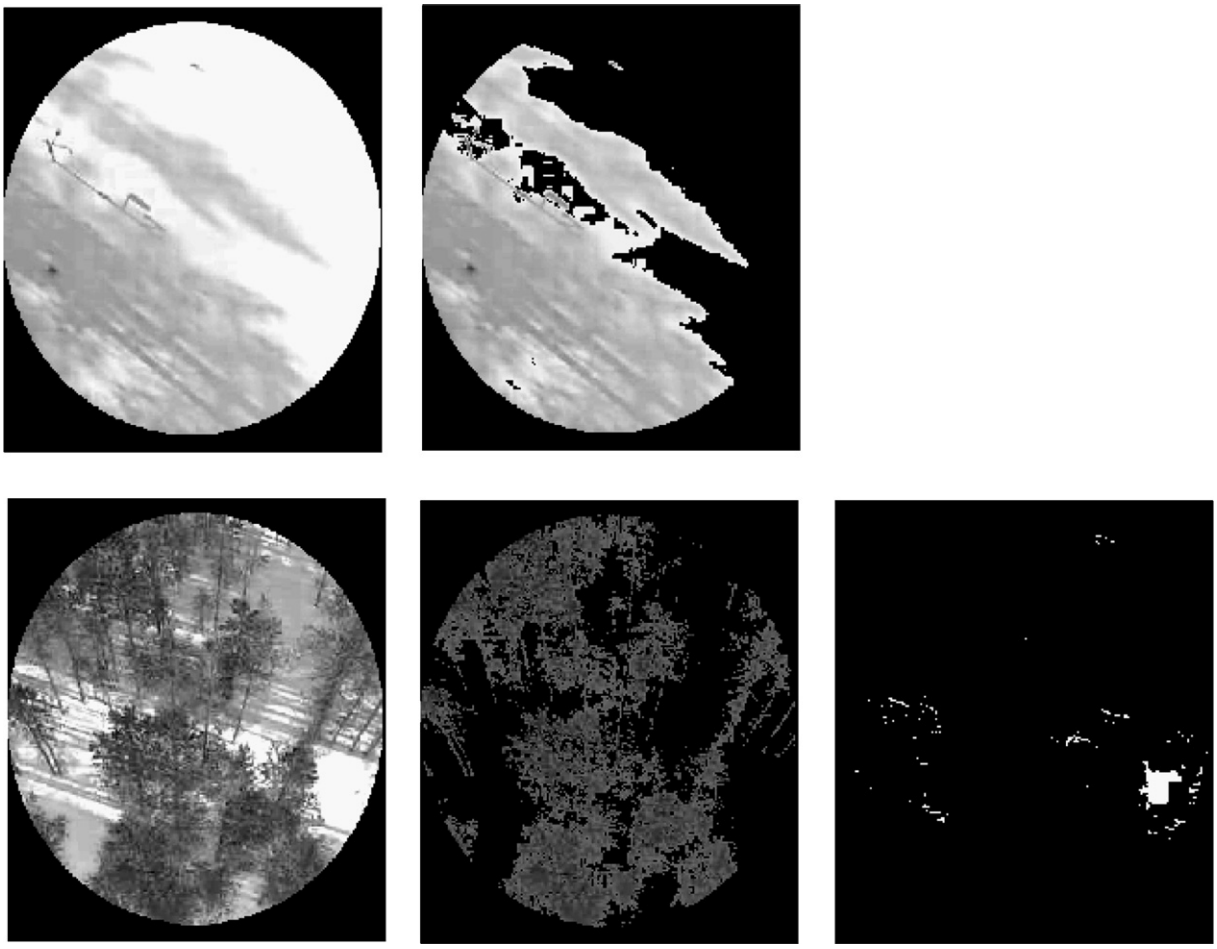

Fig. 4. (Above) Digital image and image classification for the mast-borne open area ASD measurement and (Below) for the ASD measurement of the forested area for 28 March 2008. The open area is partially shadowed by trees, the classification (above right) suggest an areal fraction of 60% for the shadowed area. The pixels from the forested area are classified to tree crowns and trunks (44%), and directly illuminated areas (1%), below middle and right respectively (thus the fraction of shadowed area is estimated to be 55%).

observation of the forested area. $\rho_{\lambda,\mathrm{trees}}$ was approximated here from the summer-time measurements of the forested area (when ground is covered by green vegetation, such as heather and lingonberry). One should note that this consideration is not ideal, for example due to the fact that multiple scattering from the snow surface strongly differs from that of green vegetation. Factors F_{direct} and F_{trees} are estimated through the analysis of concurrent high-resolution digital photographs of the area (ellipse) observed by the mast-based spectrometer, see Fig. 4.

2.4. SCAmod method accuracy assessment

SCAmod is based on a reflectance model, where the (space-borne) observed reflectance R is expressed as a function of SCA. The average

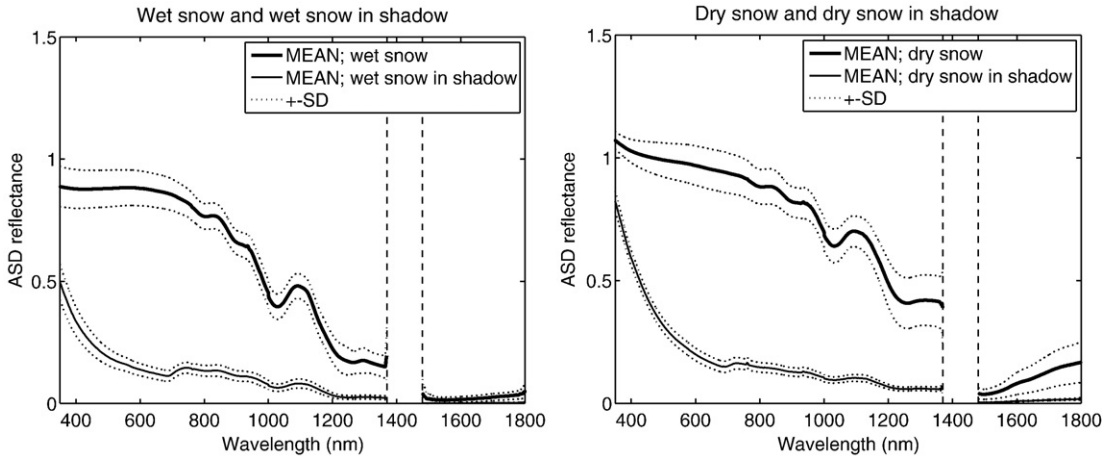

Fig. 5. (Left) Mean reflectance ± standard deviation for wet snow and (Right) mean ± standard deviation for dry snow in cases where snow is either under natural direct or diffuse illumination or fully shaded by forest trees (only including direct illumination). The wavelength area around 1400 nm is affected by a bad SNR.

apparent forest canopy transmissivity t_λ and reflectances from wet snow $\rho_{\lambda,\text{snow}}$, snow-free ground $\rho_{\lambda,\text{ground}}$, and dense forest canopy $\rho_{\lambda,\text{forest}}$ at wavelength λ, serve as model parameters (Metsämäki et al., 2005):

$$R_{\lambda,\text{obs}} = R_{\lambda,\text{obs}}(\text{SCA}) = \left(1 - t_\lambda^2\right)\rho_{\lambda,\text{forest}} + t_\lambda^2\left[\text{SCA}\rho_{\lambda,\text{snow}} + (1 - \text{SCA})\rho_{\lambda,\text{ground}}\right] \quad (4)$$

The value for effective transmissivity t_λ^2 is characteristic for each target unit area. It describes how much of the upwelling radiance is originated underneath the forest canopy. Transmissivity is determined from Eq. (4) with at-satellite reflectance observation made at full dry snow cover conditions (SCA = 1). This approach is based on the fact that under full cover dry snow conditions the required reflectance contrast between forest canopy and snow covered ground in forest openings is notable (so the estimate for transmissivity can be derived from satellite data). The applied transmissivity value also includes the effect of tree shadows. Once the transmissivity is determined, the SCA estimate for forested terrain during the spring melt period is obtained by inverting Eq. (4), as follows:

$$\text{SCA} = \frac{\frac{1}{t_\lambda^2}R_{\lambda,\text{obs}} + \left(1 - \frac{1}{t_\lambda^2}\right)\rho_{\lambda,\text{forest}} - \rho_{\lambda,\text{ground}}}{\rho_{\lambda,\text{wetsnow}} - \rho_{\lambda,\text{ground}}} \quad (5)$$

Algorithm (5) is applied for SCA mapping from space-borne data using reflectances from a single channel, typically e.g. MODIS band 3 (459–479 nm) or MERIS band 2 (436–449 nm). Additionally, NDSI or Normalized Difference Vegetation Index (NDVI) is applied in operational snow mapping to detect the disturbing effect of emerging green vegetation at the end of snow melt period. In the statistical accuracy analysis the law of error propagation can be applied. This approach provides the standard deviation of the SCA as a sum of partial derivatives (separately with respect to each model parameter) multiplied by these parameters' variances (Metsämäki et al., 2005). Therefore, the information on the variability of the model parameters is essential. These variances can be derived from experimental at-field reflectance measurements, from spectral libraries or from the space-borne earth observation data. In this work, at-ground reflectance measurements with ASD were used in order to determine variances for two reflectance contributors: wet snow and snow-free ground. The term for forest canopy reflectance was not considered in the sensitivity analyses here (one should note that the magnitude of forest canopy reflectance is only few percentages in blue wavelength often applied in snow algorithms).

The contribution of wet snow reflectance fluctuations to the standard deviation (standard error) of an SCA estimate is:

$$\text{std}(SCA)_{|\rho_{\lambda,\text{wetsnow}}} = \frac{\partial(\text{SCA})}{\partial\rho_{\lambda,\text{wetsnow}}}\text{std}\left(\rho_{\lambda,\text{wetsnow}}\right) = \frac{-\left[\frac{1}{t_\lambda^2}R_{\lambda,\text{obs}} + \left(1 - \frac{1}{t_\lambda^2}\right)\rho_{\lambda,\text{forest}} - \rho_{\lambda,\text{ground}}\right]}{\left(\rho_{\lambda,\text{wetsnow}} - \rho_{\lambda,\text{ground}}\right)^2}\text{std}\left(\rho_{\lambda,\text{wetsnow}}\right) \quad (6)$$

The contribution of ground surface reflectance fluctuations to the standard deviation (standard error) of an SCA estimate is:

$$\text{std}(\text{SCA})_{|\rho_{\lambda,\text{ground}}} = \frac{\partial(\text{SCA})}{\partial\rho_{\lambda,\text{ground}}}\text{std}\left(\rho_{\lambda,\text{ground}}\right) = \frac{\frac{1}{t_\lambda^2}R_{\lambda,\text{obs}} + \left(1 - \frac{1}{t_\lambda^2}\right)\rho_{\lambda,\text{forest}} - \rho_{\lambda,\text{snow}}}{\left(\rho_{\lambda,\text{wetsnow}} - \rho_{\lambda,\text{ground}}\right)^2}\text{std}\left(\rho_{\lambda,\text{ground}}\right) \quad (7)$$

Finally, the total error is gained as a sum of these terms:

$$\text{std}_{\text{tot}} = \sqrt{\left(\text{std}(\text{SCA})_{|\rho_{\lambda,\text{ground}}}\right)^2 + \left(\text{std}(\text{SCA})_{|\rho_{\lambda,\text{ground}}}\right))^2} \quad (8)$$

We calculated the total error for different SCA values and for three different wavelength bands related to operating space-borne optical sensors (MODIS, MERIS and AVHRR).

3. Results and discussion

Figs. 5 and 6 (Left) present the obtained standard deviation and mean reflectance spectra (biconical and hemispherical–conical reflectance factors) for wet snow, dry snow and snow-free ground, respectively. Note that the reflectance considered here refers to an *apparent* reflectance, i.e. a physical quantity observed by an Earth Observation sensor. For example, the apparent reflectance in shade stands for measured radiance (in shade) divided by the full irradiance (no shade). The corresponding quantitative information for selected wavelength bands relevant to MODIS-based snow monitoring is given in Table 3. The focused bands are essential for snow applications as MODIS band 3 (459–479 nm) is used e.g. in SYKE's operational snow map production based on *SCAmod*, while bands 4 (545–565 nm) and 6 (1628–1652 nm) are used for the Normalized Difference Snow Index (NDSI) to obtain global snow map products (Hall et al., 2002). Table 3 shows the obtained ASD reflectance values separately for direct and diffuse illumination conditions and for the combination of these two. Reflectance statistics for relevant MERIS and AVHRR wavelength

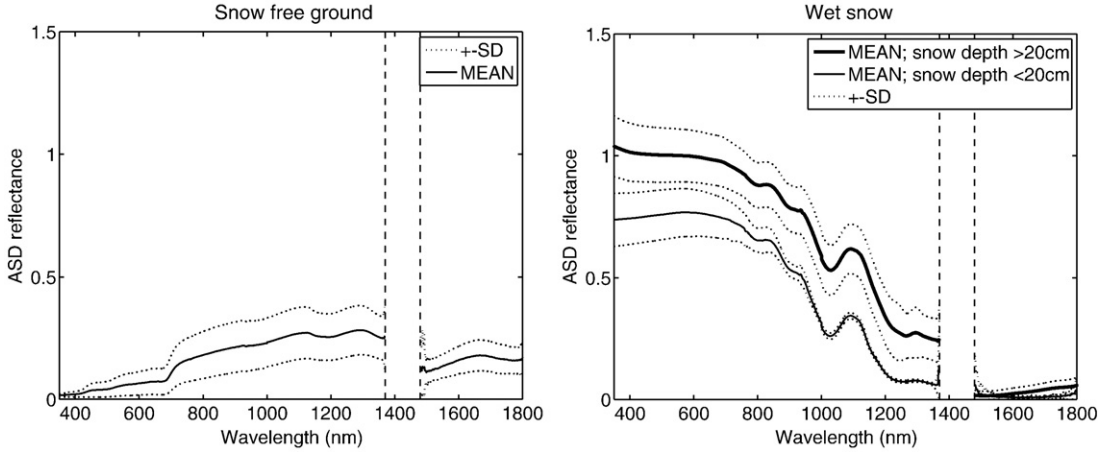

Fig. 6. (Left) Mean reflectance ± standard deviation for snow-free ground and (Right) mean reflectance ± standard deviation for wet snow in cases where snow depth is either above or below 20 cm. Results include both direct and diffuse illumination. The wavelength area around 1400 nm is affected by a bad SNR.

Table 3
Ground spectrometer derived reflectance for wet snow, dry snow and snow-free ground: mean and standard deviation under direct, diffuse and combined sunlight illumination conditions.

Direct illumination	No. of obs.	ASD 459–479 nm		ASD 545–565 nm		ASD 1628–1652 nm	
		Mean	SD	Mean	SD	Mean	SD
Wet snow	450	0.95	0.09	0.94	0.10	0.03	0.01
Dry snow	240	1.00	0.08	0.98	0.10	0.09	0.06
Snow-free ground	120	0.03	0.02	0.04	0.02	0.14	0.05
Wet snow, snow depth >20 cm	450	0.95	0.09	0.94	0.10	0.03	0.01
Wet snow, snow depth <20 cm	–	–	–	–	–	–	–
Wet snow, in shadow	180	0.22	0.04	0.16	0.03	0.00	–
Dry snow, in shadow	90	0.38	0.03	0.24	0.03	0.01	0.00
Diffuse illumination	No. of obs.	Mean	SD	Mean	SD	Mean	SD
Wet snow*	840	0.89	0.08	0.90	0.07	0.02	0.02
Dry snow	190	1.00	0.02	0.98	0.03	0.11	0.04
Snow-free ground	210	0.04	0.03	0.07	0.05	0.19	0.06
Wet snow, snow depth >20 cm	750	1.04	0.12	1.04	0.10	0.03	0.03
Wet snow, snow depth <20 cm	90	0.75	0.10	0.77	0.10	0.01	0.01
Direct and diffuse illumination	No. of obs.	Mean	SD	Mean	SD	Mean	SD
Wet snow*	1290	0.88	0.08	0.88	0.07	0.02	0.01
Dry snow	430	1.00	0.06	0.98	0.08	0.10	0.05
Snow-free ground	330	0.04	0.03	0.06	0.04	0.17	0.06
Wet snow, snow depth >20 cm	1270	1.00	0.11	1.00	0.11	0.03	0.02
Wet snow, snow depth <20 cm	90	0.75	0.10	0.77	0.10	0.01	0.01

The used wavelengths correspond to MODIS bands 3 (459–479 nm), 4 (545–565 nm) and 6 (1628–1652 nm).
*Average values for classes: wet snow depth >20 cm and wet snow depth <20 cm (root mean squared value in case of standard deviation).

bands are given in Table 4, respectively. The grain size range in the results of Fig. 5, and those of Tables 3 and 4 was 0.5–3.5 mm (mean of maximum diameter) for wet snow and 0.2–2 mm for dry snow. Snow depth distribution was 0.5–73 cm for wet snow and 54–84 cm for dry snow. As wet snow case includes several sub-cases, such as very shallow snowpack, we calculated weighted standard deviation and mean in order to obtain representative average wet snow reflectance (the weighted values are presented in Tables 3 and 4). In order to obtain the snow-free ground reflectance spectrum presented in Fig. 6 (Left), ASD observations from typical boreal forest understorey ground targets were averaged, such as mixture of low shrubs and grasses, heather, lichen, moss, lingonberry and forest litter (from measurements carried out directly after the snow melt).

The results indicate that in general, for visible wavelengths, the overall reflectance of dry snow is only slightly higher than that of wet snow, but the difference is significant in NIR and SWIR wavelengths especially for thick snow (with no contribution from the underlying soil). This coincides well with the results by Odermatt et al. (2005). Likewise, measurements by Li and Zhou (2004) indicate that with low sun and nadir view geometry, visible reflectance (HDRF) of both large and fine grained snow is close to 1, but at NIR wavelengths reflectance of larger grains is clearly lower. We also compared the spectra collected either under direct or under diffuse illumination and found that for selected wavelengths used in this study, the difference is small: the highest differences in the mean values were found for wet snow indicating a shift of 6%-units at the MODIS band of 459–479 nm (a relative difference of 6.5%), refer to Table 3 (direct and diffuse illumination). With different combinations of large/fine-grained and wet/dry snow, there was no observable difference. Thus, we calculated the overall standard deviation and mean for wet and dry snow from both direct and diffuse cases in order to obtain a more comprehensive data set to represent the melting season conditions presumed by *SCAmod*. These values are also given in Table 3.

Tables 3 and 4 also indicate that the standard deviations of observed reflectances for diffuse and direct illumination conditions do not differ significantly in general. This is an important notice, as it suggests that the variance in observations is due to the variability of in target characteristics, not due to the varying sun zenith angle (the variance observed under diffuse conditions cannot result from the changes in the sun zenith angle).

In Fig. 6 (Right), standard deviation and mean of shallow and thick wet snow are compared. This is an important aspect concerning the SCA estimation as towards the end of the melting season shallow snow conditions are usually predominant and the percentage of patchiness increases. The results show that under snow depths less than 20 cm the reflectance values decrease significantly. Also snow optical depth (and thus transmissivity through snowpack), which is related to snow density, depth, grain size and wavelength in concern, decreases with decreasing snow depth. The results in Fig. 6 clearly show that snow depth has a strong effect on the observed snow reflectance, in fact even much more significant than that of snow grain size. This was observed from the measurements by comparing data with different grain sizes and wetnesses for all snow depths. Snow depth was the only factor explaining the behaviour. Note that in Figs. 5 and 6, the data at wavelengths around 1400 nm was removed due to an insufficient signal to noise ratio (SNR).

Fig. 7 shows how the standard deviation of reflectance behaves for wet snow and snow-free ground in wavelengths below 1000 nm. Since an SCA-estimation method should be as much invariant to fluctuations of reflectances as possible, these data are very useful in choosing the optimal wavelengths to be applied. The coefficient of variation (SD/mean ratio) also given in Fig. 7 provides us valuable information for this judgement. For example, in the case of *SCAmod*, those satellite-sensor bands for which we obtained the smallest coefficients of variation both for wet snow and snow-free ground, are the most applicable and will minimize the error in the SCA estimation (note that this investigation does not discuss the spectral effects of atmospheric disturbances nor the performance of atmospheric corrections). Again, as *SCAmod* uses single band reflectances, we

Table 4
Ground spectrometer derived reflectance for wet snow, dry snow and snow-free ground: mean and standard deviation under direct, diffuse and combined sunlight illumination conditions.

Direct illumination	No. of obs.	ASD-derived MERIS 436–449 nm		ASD-derived AVHRR 580–680 nm	
		Mean	SD	Mean	SD
Wet snow	450	0.96	0.09	0.93	0.10
Dry snow	240	1.01	0.08	0.96	0.10
Snow-free ground	120	0.03	0.01	0.05	0.02
Wet snow, snow depth >20 cm	450	0.96	0.09	0.93	0.10
Wet snow, snow depth <20 cm	–	–	–	–	–
Wet snow, in shadow	180	0.26	0.05	0.13	0.02
Dry snow, in shadow	90	0.45	0.03	0.18	0.02
Diffuse illumination	No. of obs.	Mean	SD	Mean	SD
Wet snow*	840	0.89	0.08	0.89	0.07
Dry snow	190	1.01	0.02	0.96	0.04
Snow-free ground	210	0.04	0.03	0.08	0.06
Wet snow, snow depth >20 cm	750	1.04	0.12	1.03	0.09
Wet snow, snow depth <20 cm	90	0.75	0.10	0.76	0.09
Direct and diffuse illumination	No. of obs.	Mean	SD	Mean	SD
Wet snow[a]	1290	0.88	0.08	0.87	0.07
Dry snow	430	1.01	0.06	0.96	0.08
Snow-free ground	330	0.03	0.02	0.07	0.05
Wet snow, snow depth >20 cm	1270	1.01	0.11	0.99	1.10
Wet snow, snow depth <20 cm	90	0.75	0.10	0.76	0.09

The used wavelengths correspond to MERIS band 2 (436–449 nm) and AVHRR band 1 (580–680 nm).
[a] Average values for classes: wet snow depth >20 cm and wet snow depth <20 cm (root mean squared value in case of standard deviation).

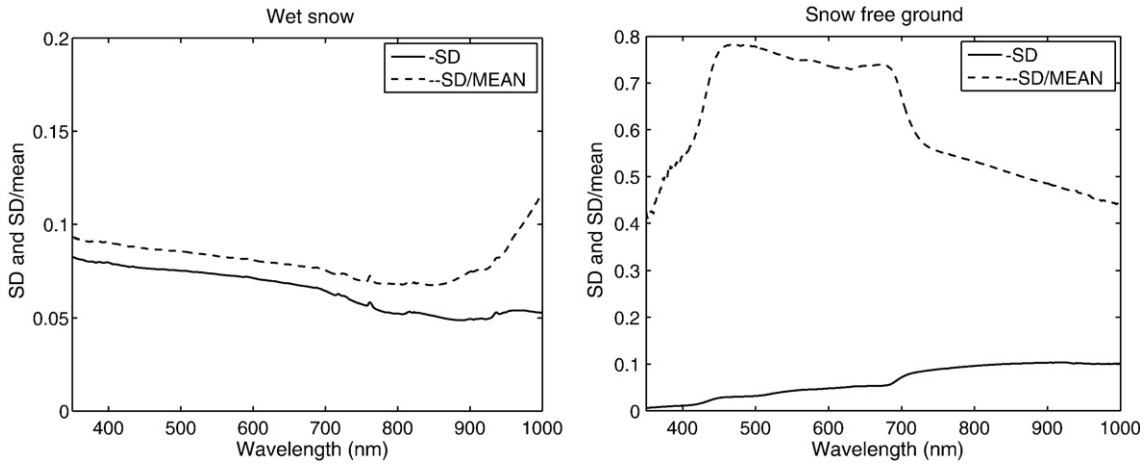

Fig. 7. (Left) Standard deviation and the coefficient of variation of reflectance (standard deviation/mean) for wet snow and (Right) snow-free ground.

focused on the selected wavelength areas in contrast to Painter et al. (2003), who focus on wide spectrum to consider the reflectance variation. According to the results in Fig. 7, wavelengths between 450 nm and 700 nm exhibit a high variability for the reflectivity of snow-free ground reducing their feasibility to wet snow detection. In contrast to that, the coefficient of variation for wet snow reflectance decreases with increasing wavelength. However, the practical usability of NIR bands during spring-melt is deteriorated by the effect of green vegetation hampering the difference in signal between snow and snow-free ground. The blue wavelengths correspond to MODIS band 3 (459–479 nm) and MERIS band 2 (436–449 nm). The usability of NIR bands is deteriorated by the effect of green vegetation hampering the difference in signal between snow and snow-free ground.

Figs. 8 and 9 show the behaviour of the statistical error contribution to SCA estimation performance due to the spatial and temporal variability of wet snow and snow-free ground reflectance. The results are obtained for *SCAmod* applying Eqs. (6)–(8) for the collected ASD reflectance data set. Again, wavelengths related to MODIS, MERIS and AVHRR bands are in focus. In Fig. 8, the standard error for SCA estimate as a function of SCA is presented due to wet snow reflectance variability only (Left) and due to snow-free ground reflectance variability only (Right). The behaviour of standard error in both cases is very logical: when wet snow reflectance is accounted for, the error increases together with increasing SCA, and when snow-free area is accounted for, the error is highest when the ground has no snow, decreasing with increasing SCA. The results of Fig. 8 are calculated by inserting Eq. (4) to either Eq. (6) or (7). Thus, the effect of forests is negligible in the error behaviour depicted. That is, these error contributors are not affected by the forest canopy characteristics. Results depicted in Fig. 8 are combined in Fig. 9 by applying Eq. (8). Thus, Fig. 9 illustrates the total standard error (Left) and total relative standard error (Right) for different fractions of snow coverage. The results show that although the reflectances of wet snow and snow-free ground do have significant variation, their influence to the actual SCA-estimate is tolerable, the maximum total error being 12%-units, depending on the value of SCA. The relative errors also show a satisfying accuracy; less than 20% for most of the SCA-cases (the increase of the relative error towards low SCA-values is insignificant as the absolute SCA-level is very small). It is also worth noting that the gained standard errors, when only wet snow and snow-free ground fluctuations are concerned, are independent from the apparent forest transmissivity.

However, forest cover is a major disturbing factor in snow monitoring with satellite sensors, since forests block the visibility from the snow surface to satellite sensor and since shadows of the trees decrease the reflectance observed above the forest canopy. This is difficult to accurately consider for varying sun and view zenith angles in models such as Eq. (4). Additionally, forest canopy (crowns and trunks) reflects a part of incoming radiation, though a very small percentage in blue to green wavelengths, such as MODIS bands 3 (459–479 nm) and 4 (545–565 nm), and MERIS band 2 (436–449 nm). Nevertheless, as *SCAmod* is based on Eq. (4), the apparent (two-way) forest canopy transmissivity considers and reduces the blocking effect

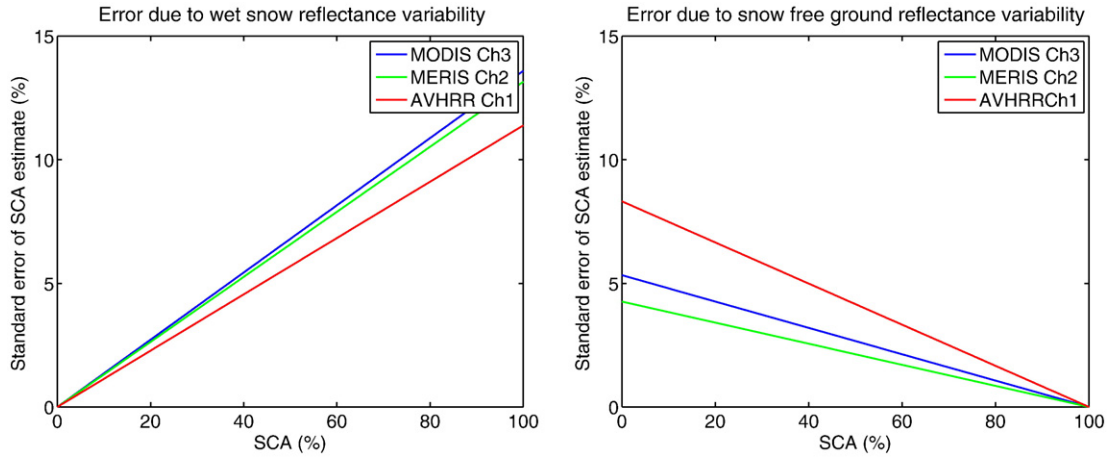

Fig. 8. (Left) The standard error of SCA estimation due to wet snow reflectance variability and (Right) snow-free ground reflectance variability. The error is estimated using wavelengths corresponding to MODIS band 3 (459–479 nm), MERIS band 2 (436–449 nm) and AVHRR band 1 (579–681 nm).

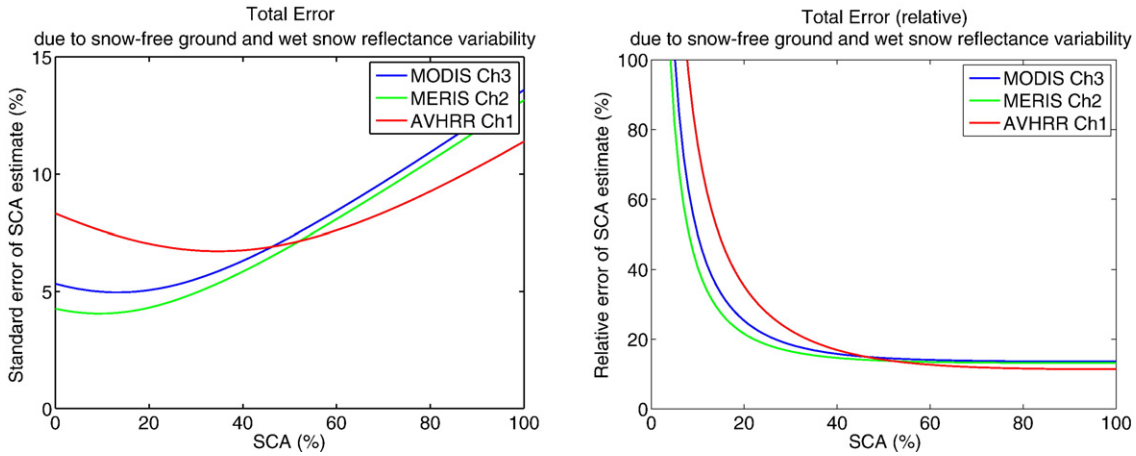

Fig. 9. (Left) The standard error (%-units) of SCA estimation due to both wet snow and snow-free ground reflectance variability. The error is estimated using wavelengths corresponding to MODIS band 3 (459–479 nm), MERIS band 2 (436–449 nm) and AVHRR band 1 (579–681 nm). (Right) The relative error (total error divided by SCA) due to both wet snow and snow-free ground reflectance variability.

of forest canopy as well as tree shadowing effects. In this study, the absolute effect of forest cover on scene reflectance was demonstrated with mast-based ASD-observations. In practise, mast-based spectrometer measurements were simulated with linear spectral mixing of ground-based ASD reflectances. This enabled the investigation of scene reflectances observed above the tree cover.

The scene reflectance was modelled using Eq. (3a) for the forest opening also measured with the mast-based spectrometer. The same was repeated for the forested area by applying Eq. (3b). The image analysis of data shown in Fig. 4 indicated that pine tree shadows covered a fraction of 60% of the spectrometer footprint during the mast-based measurement of the open area. In case of the forested area, the areal fractions of different target constitutes were: 43.5% for the tree shadows, 55.3% for the crowns/trunks and 1.3% for the directly illuminated snow cover. This information accompanied with dry snow reflectance and tree shadow reflectance data (examples for certain wavelengths given in Table 3 were used as input to (3a and 3b). For the forested area (3b) the crown reflectance was approximated by the mast-based summer-time measurements of the forested target area (assuming that ground reflectance is close to forest canopy reflectance).

The resulting reflectance spectrum simulation is presented in Fig. 10. Fig. 10 also depicts the actual observation with the mast-based spectrometer indicating a higher level of reflectance for the visible wavelengths, but spectrally an analogous response. Figs. 4 and 10 demonstrate the strong effect of tree cover even for forest openings, which has to be considered by snow monitoring algorithms if they are applied to forested regions, such as northern Finland. In case of *SCAmod* these effects are primarily considered by introducing the apparent forest canopy transmissivity. The other evident alternative is the use of spectral unmixing techniques in SCA estimation to consider the effects of tree shadows, blocking by tree canopy and the influence of crown/trunk reflectance, thus inversion of Eqs. (3a and 3b). However, this requires detailed structural forest canopy *a priori* information for estimating different target type coverage fractions, i.e. such information as that demonstrated in Fig. 4.

The possible reasons for the reflectivity difference between the predicted and observed scene reflectance factor in Fig. 10 include the small difference in the imaging geometry. The mast-based spectrometer observation of the forest opening was performed for a forward scattering direction with an azimuth angle difference of 125° between the directions of the Sun and spectrometer measurement head, and additionally, the spectrometer was tilted 11° off the nadir. In case of the forested target area, the scattering geometry was slightly towards the backward direction (azimuth angle difference of 70°). In case of observations with portable spectrometer the measurement direction

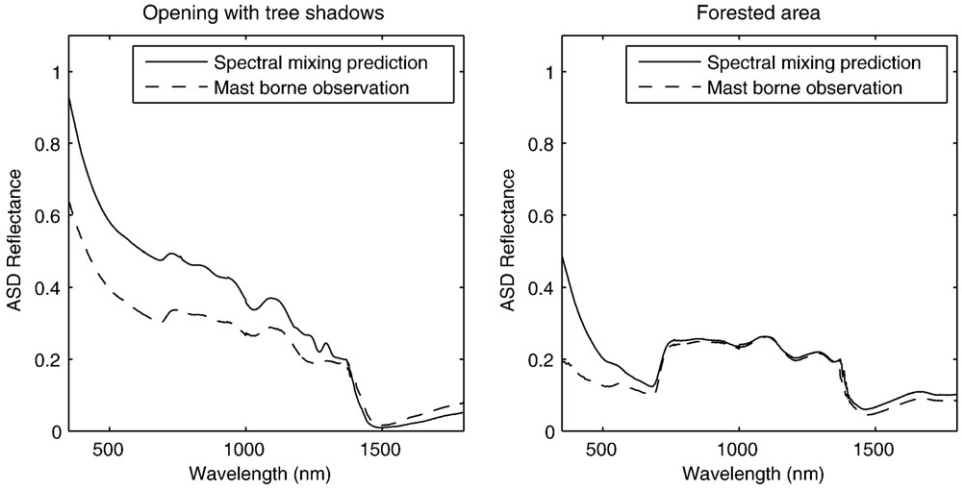

Fig. 10. (Left) Observed and predicted reflectance factor of a dry snow covered open area shadowed by pine trees and (Right) of a forested area. Measurements are carried out by the mast-borne ASD spectrometer on 28 March 2008. The corresponding prediction according to (3) is based on spectra measured by the ground-based portable ASD-system. The fraction of shadowed area is determined from Fig. 4. The dry snow and shadowed snow spectra correspond to mean observations (see Tables 3, 4 and Fig. 5).

was towards the nadir. The difference in the Sun elevation angle was marginal (slightly varying in the field spectrometer data set, refer to Table 2). Another possible reason for the difference in reflectance level may arise from the target geometry. Point-wise field spectrometer measurements represent small areas with a diameter of 20 cm, see Table 2. Mast-borne measurements are collected from a larger region (ellipse with main axes of 16.0 and 14.7 m), which include some surface undulations. As a consequence, Fig. 10 suggests that the absolute level of scene reflectance at visible wavelengths cannot be directly simulated with spectral mixing of field spectrometer-derived reflectance values.

4. Summary and conclusions

In this work, the variability of ground reflectance was investigated in order to assess the feasibility of satellite sensors to the mapping of snow covered area in the boreal forest zone. The results obtained here suggest certain requirements for space borne instruments applied to snow cover mapping. First of all, snow algorithm works best for visible wavelengths, as in this region, snow reflectance is most invariant to snow physical properties (e.g. grain size). From ASD-measurements, we found that using wavelengths at 400–480 nm or 700–800 nm, the lowest standard deviation of wet snow spectra was gained. However, in 700–800 nm region, the effect of green vegetation hampers the distinguishing of snow; therefore we concluded that when a single channel algorithm (such as *SCAmod*) is applied wavelengths 400–480 nm also with a very low standard deviation of reflectance variation, are most suitable for snow cover mapping. Due to the effect of atmospheric gases and aerosols into the reflectances in this region, it would be beneficial to use an atmospheric correction procedure in order to obtain surface reflectances instead of top-of-the-atmosphere reflectances. Neglecting the atmospheric effect will result to somewhat erroneous snow information; the magnitude of error is primarily dependent on the water vapour and aerosol content of the atmosphere during the image acquisitions.

We investigated the performance of the *SCAmod* method by applying ASD-derived reflectances for two of the *SCAmod* model parameters: wet snow and snow-free ground. Special focus was on the wavelengths related to MODIS, MERIS and AVHRR bands often utilized in snow detection. A standard error of about 5–7%-units was on average obtained, the maximum error of 10–12%-units occurring at full snow cover conditions. The results for MERIS and MODIS were notably better than those for AVHRR when SCA showed values below 40% suggesting that these instruments can be better used in snow mapping at the end of the melting season (which is the most essential period concerning hydrological end-use applications).

The investigation also demonstrates the feasibility of surface reflectance observations to predict scene reflectance characteristics actually observed by space-borne instruments. Combining the actual satellite observations with the ground-based data given in this paper is a topic of ongoing research and publication. The data presented here is also scheduled to be used in similar kind of analysis for NDSI as what is done here for *SCAmod*. The future work will further utilize the reflectance measurements of forest canopy, using spectrometer placed on the mast above the tree height. The collected data will be used in the further accuracy analysis of *SCAmod* and in the algorithm optimization. In order to derive the statistical accuracy of the apparent transmisivity, additional dry snow (illuminated and shadowed) reflectance measurements, together with forest canopy measurements, are required.

Acknowledgements

This work has been supported by the SNOW-CLIM (Snow Mapping of Boreal and Sub-Arctic Zones: Earth Observation Data-Based Multi-Source Information Systems and Application to Climatic Studies) project funded by the Academy of Finland. The work has been also supported by Interreg IIIA Nordkalotten-program project NorSEN (Nordkalotten Satellite Evaluation co-operation Network), http://norsen.fmi.fi/.

References

Anttila, S., Metsämäki, S., Pulliainen, J., & Luojus, K. (2005). From EO data to snow covered area end products using automated processing system. *Proceedings of the IEEE 2005 International Geoscience and Remote Sensing Symposium (IGARSS'05), Harmony Between Man and Nature, 25–29 July 2005, Seoul Korea, 1947–1950*.

Aoki, T., Aoki, T., Fukabori, M., Hachikubo, A., Tachibana, Y., & Nishio, F. (2000). Effects of snow physical parameters on spectral albedo and bidirectional reflectance of snow surface. *Journal of Geophysical Research*, *105*(D8), 10,219—10,236.

Barry, R. G., Armstrong, R., Callaghan, T., Cherry, J., Gearheard, S., Nolin, A., et al. (2007). Snow. *Global Outlook for Ice and Snow* (pp. 39—62). : UNEP Available at http://www.unep.org/geo/geo_ice/PDF/full_report_LowRes.pdf

Colbeck, S., Akitaya, E., Armstrong, R., Gubler, H., Lafeuille, J., Lied, K., et al. (1990). *The international classification for seasonal snow on the groundWorking Group on Snow Classification*. (pp. 23) Available at www.crrel.usace.army.mil/techpub/CRREL_-Reports/reports/Seasonal_Snow.pdf

FAO (2003). Forest area statistics. Available at http://www.fao.org/forestry/site/32185/en/fin (Accessed 6 February 2008).

Hall, D., Riggs, G. A., Salomonson, V. V., DiGirolamo, N. E., & Bayr, K. J. (2002). MODIS snow-cover products. *Remote Sensing of Environment*, *83*, 181—194.

Härmä, P., Teiniranta, R., Törmä, M., Repo, R., Järvenpää, E., & Kallio, M. (2004). Production of CORINE2000 land cover data using calibrated LANDSAT 7 ETM satellite image mosaics and digital maps in Finland. *Proceedings of the IEEE 2004 International Geoscience and Remote Sensing Symposium (IGARSS'04), Science for Society: Exploring and Managing a Changing Planet, 20–24 September 2004, Anchorage Alaska USA* (pp. 2703—2706).

Jaagus, J. (1997). The impact of climate change on the snow cover pattern in Estonia. *Climatic Change*, *36*, 65—77.

Jylhä, K., Tuomenvirta, H., & Ruosteenoja, K. (2004). Climate change projections for Finland during the 21st century. *Boreal Environment Research*, *9*, 127—152.

Kitaev, L., Førland, E., Razuvaev, V., Tveito, O. E., & Krueger, O. (2005). Distribution of snow cover over Northern Eurasia. *Nordic Hydrology*, *36*, 311—319.

Kitaev, L., Kislov, A., Krenke, A., Razuvaev, V., Martuganov, R., & Konstantinov, I. (2002). The snow cover characteristics of northern Eurasia and their relationship to climatic parameters. *Boreal Environment Research*, *7*, 437—445.

Kokhanovsky, A. A., Aoki, T., Hachikubo, A., Hori, M., & Zege, E. P. (2005). Reflective properties of natural snow: Approximate asymptotic theory versus *in situ* measurements. *IEEE Transactions on Geoscience and Remote Sensing*, *43*, 1529—1535.

Kuusisto, E. (1984). Snow accumulation and snowmelt in Finland. *Publications of the Water Research Institute*, *vol. 55*. (pp. 149)Helsinki: National Board of Waters.

Li, S., & Zhou, X. (2004). Modelling and measuring the spectral bidirectional reflectance factor of snow-covered sea ice: an intercomparison study. *Hydrological processes*, *18*, 3559—3581.

Lundberg, A., & Halldin, S. (2001). Snow measurement techniques for land-surface-atmosphere exchange studies in boreal landscapes. *Theoretical and Applied Climatology*, *70*, 215—230.

Matzl, M., & Schneebeli, M. (2006). Measuring specific surface area of snow by near-infrared photography. *Journal of Glaciology*, *52*(179), 558—564.

Mellander, P. -E., Löfvenius, M. O., & Laudon, H. (2007). Climate change impact on snow and soil temperature in boreal Scots pine stands. *Climatic Change*, *85*, 179—193.

METLA (2007). *Finnish Statistical Yearbook of Forestry* (pp.149) : Finnish Forest Research Institute.

Metsämäki, S., Anttila, S. T., Huttunen, J. M., & Vepsäläinen, J. A. (2005). A feasible method for fractional snow cover mapping in boreal zone based on a reflectance model. *Remote Sensing of Environment*, *95*, 77—95.

Metsämäki, S., Huttunen, M., & Anttila, S. (2004). The operative remote sensing of snow covered area in a service of hydrological modeling in Finland. *Proceedings of the 23rd Symposium of the European Association of Remote Sensing Laboratories (EARSeL), Remote Sensing in Transition, 2–5 June 2004, Rotterdam Belgium* (pp. 219—225).

Nolin, A. W., & Dozier, J. (1993). Estimating snow grain-size using AVIRIS data. *Remote sensing of Environment*, *44*(2–3), 231—238.

Nolin, A. W., & Dozier, J. (2000). A hyperspectral method for remotely sensing the grain size of snow. *Remote Sensing of Environment*, *74*, 207—216.

Odermatt, D., Schläpfer, D., Lehning, M., Schwikowski, M., Kneubühler, M., & Itten, K. I. (2005). Seasonal study of directional reflectance properties of snow. *European Association of Remote Sensing Laboratories EARSeL eProceedings 4, 2/2005* (pp. 203—214). Available at http://las.physik.uni-oldenburg.de/eProceedings/vol204_202/204_202_odermatt201.pdf

Oksanen, T. (1999). Suomen lumipeitteen alueellinen vaihtelu (p. 65): Master's thesis. University of Helsinki, Department of Physical Sciences. Available at http://ethesis.helsinki.fi (In Finnish).

Painter, T. H., & Dozier, J. (2004). Measurements of the hemispherical-directional reflectance of snow at fine spectral and angular resolution. *Journal of Geophysical Research*, *109*, D18115.

Painter, T. H., Dozier, J., Roberts, D. A., Davis, R. E., & Green, R. O. (2003). Retrieval of subpixel snow-covered area and grain size from imaging spectrometer data. *Remote Sensing of Environment*, *85*, 64—77.

Painter, T. H., Molotch, N. P., Cassidy, M., Flanner, M., & Steffen, K. (2007). Contact spectroscopy for the determination of stratigraphy of snow grain size. *Journal of Glaciology*, *53*(180), 121—127.

Painter, T. H., Roberts, D. A., Green, R. O., & Dozier, J. (1998). The effect of grain size on spectral mixture analysis of snow-covered area from AVIRIS data. *Remote Sensing of Environment*, *65*, 320—332.

Rosenthal, W. (1996). Estimating alpine snow cover with unsupervised spectral unmixing. *Proceedings of the IEEE 1996 International Geoscience and Remote Sensing Symposium (IGARSS 1996), 27–31 May 1996, Lincoln Nebraska USA* (pp. 2252—2254).

Räisänen, J. (2008). Warmer climate: less or more snow? *Climate Dynamics*, *30*, 307—319.

Salomonson, V. V., & Appel, I. (2004). Estimating fractional snow cover from MODIS using the normalized difference snow index. *Remote Sensing of Environment*, *89*, 351—360.

Sandmeier, S., Müller, C., Hosgood, B., & Andreoli, G. (1998). Sensitivity analysis and quality assessment of laboratory BRDF data. *Remote Sensing of Environment*, *64*(2), 176—191.

Schaepman, M. E., Green, R. O., Ungar, S. G., Curtiss, B., Boardman, J., Plaza, A. J., et al. (2006). The future of imaging spectroscopy—Prospective technologies and applications. *Proceedings of the IEEE 2006 International Geoscience and Remote Sensing Symposium (IGARSS'06) and 27th Canadian Symposium on Remote Sensing, July 31–August 4, 2006, Denver Colorado USA, 2005–2009*.

Schaepman-Strub, G., Schaepman, M. E., Painter, T. H., Dangel, S., & Martonchik, J. V. (2006). Reflectance quantities in optical remote sensing—Definitions and case studies. *Remote Sensing of Environment*, *103*, 27—42.

Sturm, M., Holmgren, J., & Liston, G. E. (1995). A seasonal snow cover classification system for local to global applications. *Journal of Climate*, *8*, 1261—1283.

Sukuvaara, T., Pulliainen, J., Kyrö, E., Suokanerva, H., Heikkinen, P., & Suomalainen, J. (2007). Reflectance spectroradiometer measurement system in 30 meter mast for validating satellite images. *Proceedings of the IEEE 2007 International Geoscience and Remote Sensing Symposium (IGARSS), Sensing And Understanding Our Planet, 23–27 July 2007, Barcelona Spain* (pp. 1524—1528).

Walsh, J. E. (2005). Cryosphere and hydrology. *Arctic Climate Impact Assessment* (pp. 183—242) : Cambridge University Press Available at http://www.acia.uaf.edu

Warren, S. G. (1982). Optical properties of snow. *Reviews of Geophysics and Space Physics*, *20*, 67—89.

Vavrus, S. (2007). The role of terrestrial snow cover in the climate system. *Climate Dynamics*, *29*, 73—88.

Vikhamar, D., & Solberg, R. (2003). Snow-cover mapping in forests by constrained linear spectral unmixing of MODIS data. *Remote Sensing of Environment*, *88*, 309—323.

Vikhamar, D., & Solberg, R. (2003). Subpixel mapping of snow cover in forests by optical remote sensing. *Remote Sensing of Environment*, *84*, 69—82.

Wiscombe, W. J., & Warren, S. G. (1980). A model for the spectral albedo of snow. I: pure snow. *Journal of the Atmospheric Sciences*, *37*, 2712—2733.

Xie, Y., Yang, P., Gao, B. -C., Kattawar, G. W., & Mishchenko, M. I. (2006). Effect of ice crystal shape and effective size on snow bidirectional reflectance. *Journal of Quantitative Spectroscopy & Radiative Transfer*, *100*, 457—469.